Kinematics of a 6-RUU Parallel Robots with Reconfigurable Platforms

Guanglei Wu and Huimin Dong

School of Mechanical Engineering, Dalian University of Technology, Dalian 116024, China, e-mail: gwu@dlut.edu.cn; donghm@dlut.edu.cn

Abstract. This paper presents a HEXA parallel robots with reconfigurable platforms of Schönflies motion and its kinematic study. Four limbs of the robot forms a fully parallel Schönflies-motion robot, with a six-bar linkage to locate the second end-effector. The second end-effector is constrained by a four-bar linkage subject to a prescribed pose of the first end-effector as well as the two remaining limbs. The kinematic issues of the robot, i.e., the inverse geometry, kinematic constraints of the reconfigurable platforms and Jacobian matrices, are studied. Some transmission indices are defined to investigate the robot performance and the reachable workspace for both end-effectors are identified. The isocontours of the transmission indices over the regular workspace are visualized for graphical presentation of the robot's transmission performance.

Key words: Pick-and-place robot, Schönflies motion, HEXA, reconfigurable platforms.

1 Introduction

High-speed parallel robots with Schönflies motion are dedicated to fast pick-and-place (PnP) operations, serving in the light industries of food handling and electronic board assembly, etc.. Amongst this type of robots [7, 10, 3, 14], most of them inherit the architecture from the Adept Quattro robot [1], which has a symmetrical base platform and four identical limbs.

With the increasing requirement on grasping capabilities of this type of robots, a number of fully parallel robots were modified and improved for performance enhancement. For instance, the FANUC M-3iA/6A robot [2] adopts the structure of the translational Delta robot, with three actuators mounted on the ends of the three actuated links to actuate its wrist-mechanism end-effector. To reduce the dynamic inertia, a double Delta robot was proposed by fixing all the actuators [12], towards high acceleration. This design concept was inspired by the approach of coupling two planar parallel translational robots to generate the Schönflies motion [6]. Actuation redundancy was also considered as a way to enhance the acceleration capability of the PnP robots [5] as well as reconfiguration [4]. The previous robots were improved in the kinematic or dynamic aspects, resulting in one end-effector. To

improve the PnP efficiency, a strategy is to make the robot have reconfigurable platforms to install multiple grippers. A 5-dof RRΠRR robot [8], with two translational end-effectors, was developed for electric board assembly, for which the connecting bars of the mobile platforms constitute a six-bar linkage. Sequentially, architectural modifications can be made to the previous reconfigurable platforms to generate an additional rotation around an axis of vertical direction for each end-effector, as the Schönflies motion is more and more popular in material handling.

On the basis of the design of reconfigurable platforms [8], this paper will present a HEXA [9] base 6-RUU parallel robots with reconfigurable platforms of Schönflies motion as shown in Fig. 1(a) and preliminary kinematic study. The displacement group of the mobile platforms is studied. Moreover, the reachable workspace is identified and some transmission indices are defined to investigate the robot's performance, where the isocontours of the transmission indices over the regular workspace are visualized to show the robot's transmission performance.

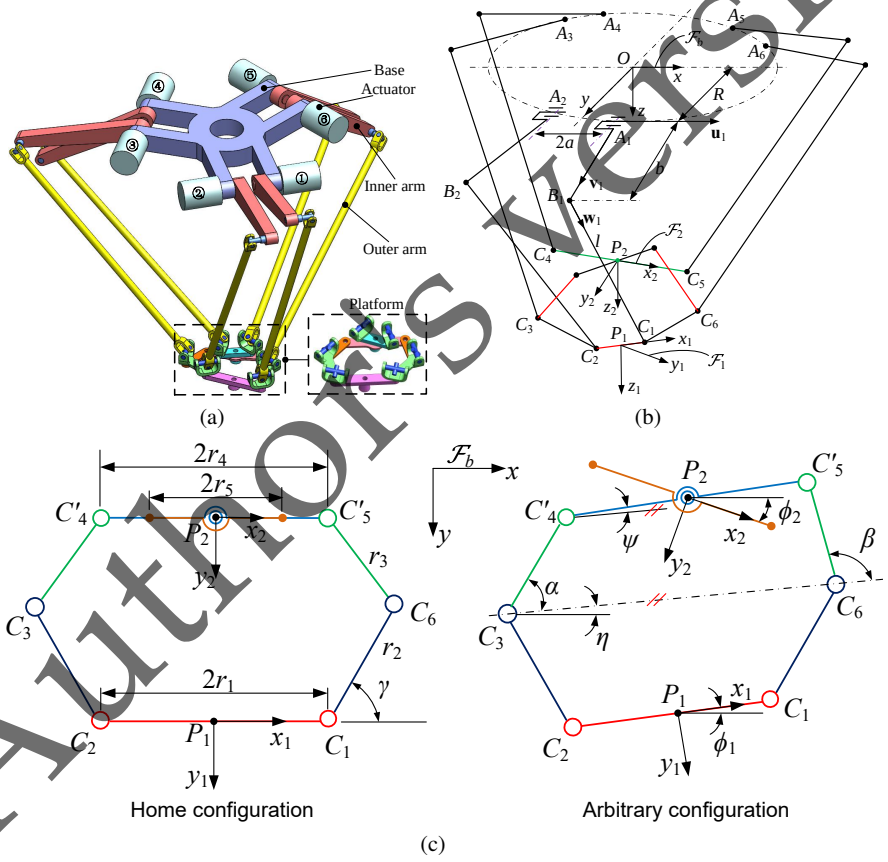

Fig. 1 The 6-RUU robot: (a) CAD model; (b) parameterization; (c) top view of the platform.

2 Manipulator Under Study and Displacement Group

The parameterizations of the robot are depicted in Figs. 1(b) and 1(c). Limbs 1 and 6 are connected by a sub-platform as well as limbs 2 and 3, which behaves similar to the articulated platform of Quattro robot [1], the rotation of the end-effector 1 being realized by their relative movements. Moreover, limbs 4 and 5 are coupled by the end-effector 2 that is located in a six-bar linkage formed by limbs 1, 2, 3 and 6.

The global coordinate frame $\mathscr{F}_b$ is built with the origin located at the geometric center of the base platform, namely, point O, where the x-axis is parallel to the axes of rotation of the first two actuated joints. The moving coordinate frames $\mathscr{F}_1$ and $\mathscr{F}_2$ are located at the geometric centers of the two end-effectors, namely, points P_1 and P_2, where x_1 and x_2-axes are parallel to the segments C_2C_1 and C_4C_5, respectively. The angle between $\mathbf{u}_i$ and x-axis is represented by μ_i, $\mu_1 = \mu_2 = 0$, $\mu_3 = \mu_4 = 2\pi/3$, $\mu_5 = \mu_6 = -2\pi/3$. Moreover, unit vectors $\mathbf{v}_i$ and $\mathbf{w}_i$ are parallel to the segments $\overline{A_iB_i}$ and $\overline{B_iC_i}$, respectively, namely, the unit vectors along the active link and parallelogram in the ith limb. Here and after, vectors $\mathbf{i}$, $\mathbf{j}$ and $\mathbf{k}$ represent the unit vectors of x-, y- and z-axis, respectively. In the following study, the vertical offsets in the platforms are supposed to be zero for convenience, as they do not affect the planar motion of the end-effector.

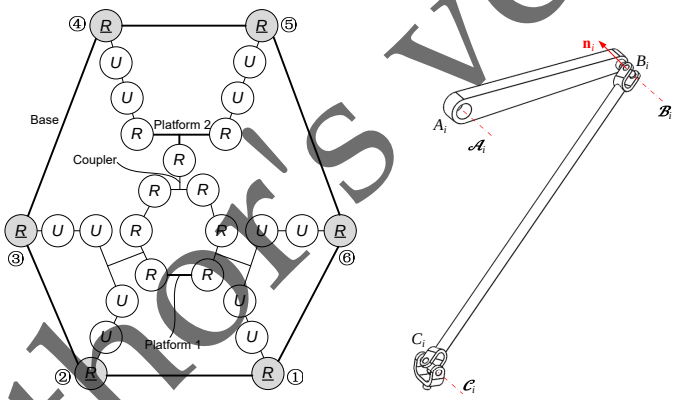

Fig. 2 The loop structure of the robot: (a) joint-and-loop graph; (b) one limb with rotational input.

Figure 2(a) depicts the joint-and-loop graph of the robot, wherein the gray and white boxes represent the actuated and passive joints, respectively. With the Group Theory, the kinematic bond $\mathscr{L}_i$ of the RUU chain in ith limb, as displayed in Fig. 2(b), is the product as below:

$$\mathscr{L}_i = \mathscr{R}(\mathscr{A}_i) \cdot \mathscr{R}(\mathscr{B}_i) \cdot \mathscr{T}(\mathbf{n}_i) \cdot \mathscr{R}(\mathscr{C}_i) = \mathscr{X}(\mathbf{u}_i) \tag{1}$$

and the kinematic bonds of the joint 1st and 6th limbs $\mathscr{L}_{16}$ is

$$\mathscr{L}_{16} = \mathscr{T} \cdot \mathscr{R}(N, \mathbf{k}) = \mathscr{X}(\mathbf{k}) \tag{2}$$

Similarly, the kinematic bonds of the 2nd and 3rd limbs $\mathscr{L}_{23}$ is $\mathscr{X}(\mathbf{k})$. Subsequently, the intersection of the subgroups for platform 1 results in a Schönflies subgroup $\mathscr{X}(\mathbf{k})$, namely, the Schönflies motion.

On the other hand, the kinematic bonds $\mathscr{L}_{45}$ of the closed loop A_4–B_4–C_4–C_5–B_5–A_5 is

$$\mathscr{L}_{45} = \mathscr{T} \cdot \mathscr{S}(N) \tag{3}$$

and the subgroups of the coupler in the closed loop six-bar linkage is $\mathscr{X}(\mathbf{k}) \cdot \mathscr{G}(\mathbf{k})$, where $\mathscr{G}(\mathbf{k})$ is the planar motion subgroup. Therefore, the intersection of all the subgroups for platform 2 leads to $\mathscr{X}(\mathbf{k}) \cdot \mathscr{G}(\mathbf{k}) \cap \mathscr{T} \cdot \mathscr{S}(N) = \mathscr{X}(\mathbf{k})$, meaning that platform 2 performs the Schönflies motion.

3 Kinematic Modeling of the Robot

3.1 Inverse Geometry

The inverse geometry problem of the robot can be readily solved from the following kinematic constraint equation:

$$\|\mathbf{c}_i - \mathbf{b}_i\| - l = 0 \tag{4}$$

To this end, the angular displacement of the ith actuated joint is solved as

$$\theta_i = 2\tan^{-1}\frac{-I_i \pm \sqrt{I_i^2 + J_i^2 - K_i^2}}{K_i - J_i} \quad \text{where} \quad \begin{cases} I_i = -2bm_{iz} \\ J_i = 2b(m_{ix}\sin\mu_i - m_{iy}\cos\mu_i) \\ K_i = \|\mathbf{m}_i\|^2 + b^2 - l^2 \end{cases} \tag{5}$$

where $\mathbf{m}_i = \begin{bmatrix} m_{ix} & m_{iy} & m_{iz} \end{bmatrix}^T = \mathbf{c}_i - \mathbf{a}_i$, and $\mathbf{a}_i$ and $\mathbf{c}_i$, respectively, are the Cartesian coordinates of points A_i and C_i in $\mathscr{F}_b$:

$$\mathbf{a}_i = \mathbf{R}_z(\mu_i)\left[(-1)^{i+1}a\mathbf{i} + R\mathbf{j}\right] \tag{6a}$$

$$\mathbf{c}_i = \begin{cases} \mathbf{p}_1 + (-1)^{i+1} r_1 \mathbf{Q}_1 \mathbf{i}, & i = 1, 2 \\ \mathbf{p}_1 + (-1)^{i} r_1 \mathbf{Q}_1 \mathbf{i} - r_2 \left[(-1)^{i+1}\cos\gamma \ \sin\gamma \ 0\right]^T, & i = 3, 6 \\ \mathbf{p}_2 + (-1)^{i+1} r_5 \mathbf{Q}\mathbf{i}, & i = 4, 5 \end{cases} \tag{6b}$$

and $\mathbf{p}_j = \begin{bmatrix} x_j & y_j & z \end{bmatrix}^T$, $j = 1, 2$, are the Cartesian coordinates of points P_j, i.e., the end-effector position, and $\mathbf{Q}_j = \mathbf{R}_z(\phi_j)$ are the rotation matrices of the end-effectors.

Moreover, the poses of the two end-effectors are kinematically constrained:

$$k_1 + k_2\cos\beta - k_3\cos\alpha - \cos\alpha\cos\beta - \sin\alpha\sin\beta = 0 \tag{7a}$$
$$\mathbf{c}_3 + \mathbf{R}_\eta\left[r_3\mathbf{R}_z(\alpha)\mathbf{i} + r_4\mathbf{R}_z(\psi)\mathbf{i}\right] - \mathbf{p}_2 = 0 \tag{7b}$$
$$\mathbf{c}_6 + \mathbf{R}_\eta\left[r_3\mathbf{R}_z(\beta)\mathbf{i} - r_4\mathbf{R}_z(\psi)\mathbf{i}\right] - \mathbf{p}_2 = 0 \tag{7c}$$

with

$$\mathbf{R}_\eta = \begin{bmatrix}\cos\eta & \sin\eta & 0\\ \sin\eta & -\cos\eta & 0\\ 0 & 0 & 1\end{bmatrix}, k_1 = \frac{\|\mathbf{c}_6 - \mathbf{c}_3\|^2 + 2r_3^2 - 4r_4^2}{2r_3^2}, k_2 = k_3 = \frac{\|\mathbf{c}_6 - \mathbf{c}_3\|}{r_3} \tag{8}$$

3.2 Kinematic Jacobian matrix and transmission index

Differentiating Eq. (4) with respect to time leads to

$$\mathbf{A}\dot{\boldsymbol{\chi}} = \mathbf{B}\dot{\boldsymbol{\theta}} \tag{9}$$

with

$$\mathbf{A} = \left[\mathbf{e}_1^T \ \ldots \ \mathbf{e}_6^T\right]^T; \quad \dot{\boldsymbol{\chi}} = \left[\dot{x}_1 \ \dot{y}_1 \ \dot{z} \ \dot{\phi}_1 \ \dot{x}_2 \ \dot{y}_2 \ \dot{\phi}_2\right]^T \tag{10a}$$
$$\mathbf{B} = \mathrm{diag}\left[h_1 \ h_2 \ \ldots \ h_6\right]; \quad \dot{\boldsymbol{\theta}} = \left[\dot{\theta}_1 \ \dot{\theta}_2 \ \ldots \ \dot{\theta}_6\right]^T \tag{10b}$$

where $\mathbf{A}$ and $\mathbf{B}$ are the forward and inverse Jacobian matrices, respectively, and

$$\mathbf{e}_i = \begin{cases}\left[\mathbf{w}_i^T \ \mathbf{w}_i^T\mathbf{s}_i \ 0_{1\times 3}\right], i = 1, 2, 3, 6\\ \left[\mathbf{0}_{1\times 2} \ w_{iz} \ 0 \ w_{ix} \ w_{iy} \ \mathbf{w}_i^T\mathbf{s}_i\right], i = 4, 5\end{cases}; \quad h_i = b\mathbf{w}_i^T(\mathbf{u}_i \times \mathbf{v}_i) \tag{11}$$

here, $\mathbf{w}_i = \left[w_{ix} \ w_{iy} \ w_{iz}\right]^T = (\mathbf{c}_i - \mathbf{b}_i)/l$, $\mathbf{s}_{1(6)} = -\mathbf{s}_{2(3)} = r_1\mathbf{Q}_1\mathbf{j}$, $\mathbf{s}_5 = -\mathbf{s}_4 = r_5\mathbf{Q}_2\mathbf{j}$.

From Eqs.(10a) and (10b), it is seen that the number of output parameters is not equal to that of input ones, for which the reason lies in the kinematic constraints of the two end-effectors.

For performance evaluation, some transmission indices will be defined, in order to accommodate the dimensional inhomogeneity of the forward Jacobian matrix due to the mixed linear and rotational motions of end-effectors.

From the determinant $|\mathbf{B}|$ of the inverse Jacobian matrix $\mathbf{B}$ below:

$$|\mathbf{B}| = \prod_{i=1}^{6} h_i = b^6 \prod_{i=1}^{6} \mathbf{w}_i^T(\mathbf{u}_i \times \mathbf{v}_i) \tag{12}$$

the input transmission index λ_i of the ith limb is defined as [13]

$$\lambda_i = |\cos\vartheta_i| = |\mathbf{w}_i^T(\mathbf{u}_i \times \mathbf{v}_i)| \in [0, 1], \quad i = 1, ..., 6 \tag{13}$$

where ϑ_i is the pressure angle [11] associated with the motion transmission, i.e., the motion transmitted from the actuated link to the parallelogram.

The limbs 1, 2, 3, 6 and the end-effector 1 determines a fully Schönflies-motion robot, for which the input and output twists are mapped by the following equation:

$$\mathbf{A}_1\dot{\boldsymbol{\chi}}_1=\mathbf{B}_1\dot{\boldsymbol{\theta}}_1;\ \mathbf{A}_1=\begin{bmatrix}\mathbf{w}_1 & r_1\mathbf{w}_1^T\mathbf{s}_1\\ \mathbf{w}_2 & r_1\mathbf{w}_2^T\mathbf{s}_2\\ \mathbf{w}_3 & r_1\mathbf{w}_3^T\mathbf{s}_3\\ \mathbf{w}_6 & r_1\mathbf{w}_6^T\mathbf{s}_6\end{bmatrix},\ \dot{\boldsymbol{\chi}}_1=\begin{bmatrix}\dot{x}_1\\ \dot{y}_1\\ \dot{z}\\ \dot{\phi}_1\end{bmatrix},\ \mathbf{B}_1=\begin{bmatrix}h_1 & & & \\ & h_2 & & \\ & & h_3 & \\ & & & h_6\end{bmatrix},\ \dot{\boldsymbol{\theta}}_1=\begin{bmatrix}\dot{\theta}_1\\ \dot{\theta}_2\\ \dot{\theta}_3\\ \dot{\theta}_6\end{bmatrix} \tag{14}$$

With the Laplace expansion, the determinant of the forward Jacobian $\mathbf{A}_1$ is [13]:

$$|\mathbf{A}_1|=2r_1(\mathbf{w}_1\times\mathbf{w}_6)\times(\mathbf{w}_2\times\mathbf{w}_3)\cdot\mathbf{s}_1 \tag{15}$$

then the output transmission index σ for the end-effector 1 is defined as

$$\sigma=|\cos\omega|=\frac{|(\mathbf{w}_1\times\mathbf{w}_6)\times(\mathbf{w}_2\times\mathbf{w}_3)\cdot\mathbf{s}_1|}{\|(\mathbf{w}_1\times\mathbf{w}_6)\times(\mathbf{w}_2\times\mathbf{w}_3)\|}\in[0,\,1] \tag{16}$$

where ω is the pressure angle amongst limbs, namely, the force transmitted from the end-effector to the passive parallelograms in the other limbs, provided that the actuated joints in these limbs are locked.

Moreover, the output transmission index for limbs 4 and 5 are defined by [14]

$$\xi_k=\frac{|\hat{\$}_{Ok}\circ\hat{\$}_{Tk}|}{|\hat{\$}_{Ok}\circ\hat{\$}_{Tk}|_{\max}}\in[0,\,1];\quad \hat{\$}_{Ok}=\begin{bmatrix}\mathbf{k}\\ r_5\mathbf{Q}_2\mathbf{i}\end{bmatrix},\hat{\$}_{Tk}=\begin{bmatrix}\mathbf{w}_k\\ b\mathbf{v}_k\times\mathbf{w}_k\end{bmatrix},k=4,5 \tag{17}$$

where $\hat{\$}_{Ok}$ and $\hat{\$}_{Tk}$ are the unit output twist screw (OTS) and transmission wrench screw (TWS) of the ith limb, respectively.

The larger value of the indices defined in Eqs. (13), (16) and (17) indicates better transmission quality and while index value 0 means singular configuration.

4 Workspace and Transmission Analysis of the Robot

The workspace of the robot under study can be obtained from Eqs. (4) and (5), either by CAD approach or numerical searching method. Here, the numerical searching method is adopted, where the geometric parameters are given in mm: $R=200$, $a=60$, $b=260$, $l=550$, $r_1=r_2=r_3=r_4=r_5=60$.

With a prescribed position of point P_1, the maximum reachable positions of the end-effector 2, namely, point P_2, are displayed in Fig. 3(a). The reachable workspace of the end-effector 1 (green) and the end-effector 2 (red) of the mobile platforms with a constant orientation $\phi_1=\phi_2=0$ are shown in Fig. 3(b) together with a fitted regular common workspace for the two end-effectors.

Figure 4 shows the transmission indices defined in previous section over the regular workspace with constant orientations. From these figures, it can be seen that the input transmission indices are larger than 0.2, which are relatively larger than

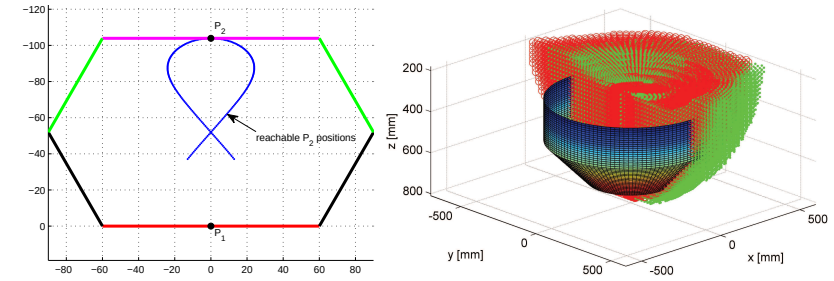

(a) (b)

Fig. 3 The workspace of the robot with $\phi_1 = \phi_2 = 0$: (a) possible positions of end-effector 2 relative to end-effector 1; (b) reachable workspace of both end-effectors.

the output transmission indices of both end-effectors. The output transmission indices of end-effector 1 which are close to 0 appear in the workspace boundaries, while some smaller indices ξ of end-effector 2 occurs inside the workspace, showing that the transmission quality for end-effector 1 are better than end-effector 2 in most region of the workspace. This means that the end-effector 2 will encounter parallel singularities inside the workspace, thus, the motors of the robot needs to be arranged for singularity-free design. Another observation is that the robot can have better transmission with Cartesian coordinates of $y \leq 0$. Moreover, the first end-effector admits a relatively larger operational workspace with transmission indices larger than LTI ≥ 0.7 for high transmission quality.

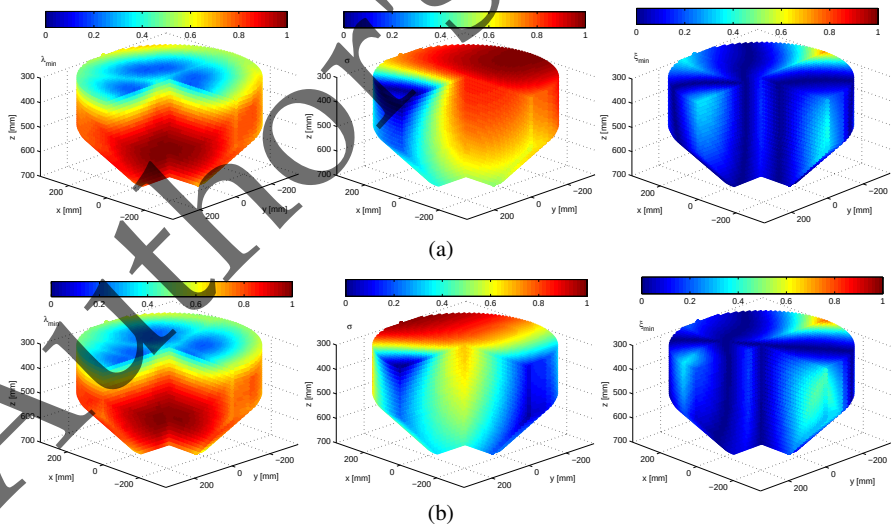

(a)

(b)

Fig. 4 Transmission indices of the robot over the regular workspace with constant orientations: (a) $\phi_1 = \phi_2 = 0$; (b) $\phi_1 = -\phi_2 = \pi/4$.

5 Conclusions

This paper presents a HEXA parallel robots with reconfigurable platforms, of which both end-effectors perform Schönflies motions. Four limbs of the robot constitute a fully parallel Schönflies-motion robot and the second end-effector is kinematically constrained by the former. The Jacobian matrices are derived to define the transmission indices and the corresponding isocontours are plotted to show the transmission quality of the translational workspace with rotational capability $\pm 45^\circ$. The first end-effector is almost free of singularity within the identified regular workspace, while the second one will encounter parallel singularities inside the workspace. In the future, singularity-free design will be conducted.

Acknowledgements The reported work is supported by the Fundamental Research Funds for the Central Universities under grant No. DUT16RC(3)068.

References

1. Adept Quattro Parallel Robots. http://www1.adept.com/main/ke/data/Archived/Quattro/sQuattro_UG.pdf
2. M-3iA Delta robot. http://www.fanuc.eu/se/en/robots/robot-filter-page/m3-series/m-3ia-6a
3. Altuzarra, O., Şandru, B., Pinto, C., Petuya, V.: A symmetric parallel Schönflies-motion manipulator for pick-and-place operations. Robotica **29**, 853–862 (2011)
4. Balmaceda-Santamaría, A., Castillo-Castaneda, E., Gallardo-Alvarado, J.: A novel reconfiguration strategy of a Delta-type parallel manipulator. Int. J. Adv. Robot. Syst. (2016)
5. Corbel, D., Gouttefarde, M., Company, O., Pierrot, F.: Actuation redundancy as a way to improve the acceleration capabilities of 3T and 3T1R pick-and-place parallel manipulators. ASME J. Mech. Robot. **2**(4), 041,002 (2010)
6. Gosselin, C., Isaksson, M., Marlow, K., Laliberté, T.: Workspace and sensitivity analysis of a novel nonredundant parallel SCARA robot featuring infinite tool rotation. IEEE Robot. Autom. Letters **1**(2), 776–783 (2016)
7. Krut, S., Nabat, V., Company, O., Pierrot, F.: A high-speed parallel robot for SCARA motions. In: IEEE Int. Conf. Robot. Autom., vol. 4, pp. 4109–4115 (2004)
8. Lambert, P.: Parallel robots with configurable platforms. Ph.D. thesis, Delft University of Technology (2013)
9. Pierrot, F., Dauchez, P., Fournier, A.: HEXA: a fast six-dof fully-parallel robot. In: Fifth Inter. Conf. Adv. Robot., pp. 1158–1163 (1991)
10. Pierrot, F., Nabat, V., Company, O., Krut, S., Poignet, P.: Optimal design of a 4-dof parallel manipulator: From academia to industry. IEEE Trans. Robot. **25**(2), 213–224 (2009)
11. Takeda, Y., Funabashi, H.: A transmission index for in-parallel wire-driven mechanisms. JSME Inter. J. Series C Mech. Syst., Mach. Elem. Manuf. **44**(1), 180–187 (2001)
12. Wu, G.: Conceptual design and analysis of a 6-axis double Delta robot towards high acceleration. In: Proc. ASIAN MMS 2016 & CCMMS 2016, pp. 389–401 (2016)
13. Wu, G.: Kinematic analysis and optimal design of a wall-mounted four-limb parallel Schönflies-motion robot for pick-and-place operations. J. Intell. Robot. Syst. (2016)
14. Wu, G., Bai, S., Hjørnet, P.: Architecture optimization of a parallel schönflies-motion robot for pick-and-place applications in a predefined workspace. Mech. Mach. Theory **106**, 148–165 (2016)